Chapter 4

CO Rovibrational Emission: A Probe of Inner Disk Structure

This chapter will be submitted to *The Astrophysical Journal* with authors C. Salyk, G. A. Blake, A. C. A. Boogert, and J. M. Brown.

4.1   Abstract

We present observations of CO rovibrational emission from a collection of T Tauri and HAe/Be stars and an analysis of emission line shapes and widths. Line shapes are consistent with an origin in a circumstellar disk atmosphere within a few AU from the parent star, although line asymmetry from some sources may be indicative of an additional inflow or outflow origin. With knowledge of disk inclination, line widths yield the inner extent of CO in the disk. We show that CO inner radii correlate well with dust inner radii and an approximate $r \propto L_\star^{1/2}$ relationship for most stars confirms that inner radii are set by dust sublimation. However, a number of stars appear to have unusually small CO inner radii, perhaps because of non-Keplerian line broadening. Additionally, high-mass HAe and Be stars have unusually large CO inner radii, which may indicate a transition in disk structure at $\sim 11\,L_\odot$. Transitional disks also have unusually large dust and CO inner radii, consistent with the idea that these disks have been dynamically cleared and may represent an advanced state of disk evolution. However, using accretion rates as a proxy for age, we find no additional correlation between CO disk radii and age.

4.2   Introduction

Observations of the inner regions ($\lesssim$ 5 AU) of circumstellar disks are essential for obtaining a complete understanding of star and planet formation. The inner disk interacts with the central star, thereby controlling the accretion and ejection of material and setting the timescale for star formation and disk evolution. In addition, inner disks are the likely birthplace of terrestrial planets. Unfortunately, however, conventional telescopes cannot resolve these regions at the distance of known star-forming clouds.

Recently, significant advancements in our understanding of inner disks have been made with two complementary techniques: IR interferometry and high-resolution spectroscopy. IR interferometry is capable of observing thermal emission from the dusty component of disks with resolutions of a few mas (probing size scales down to a few hundredths of an AU) (Millan-Gabet et al., 1999; Eisner et al., 2003; Akeson et al., 2005b; Monnier et al., 2005). High-resolution spectroscopy, on the other hand, has been used to study vibrational emission from hot gaseous molecules, specifically H_2O and CO (Najita et al., 2003; Blake and Boogert, 2004; Carr et al., 2004; Rettig et al., 2004; Brittain et al., 2003). Vibrational emission requires high temperatures and densities, which are preferentially found in inner disks, and thus allows for a focused look at these regions. In addition, observations at high spectral resolution provide spatial information because line profiles are constructed of emission from a rotating Keplerian disk. Both IR interferometry and high-resolution spectroscopy have resulted in successful observations of both T Tauri and Herbig Ae/Be stars with a range of masses, luminosities, and characteristics.

As a result of the extensive and varied IR interferometric studies, a number of patterns have emerged that have improved our understanding of inner disk structure. Firstly, it was noticed that standard, optically thick accretion disk models (such as outlined by Hillenbrand et al. (1992)) fail to simultaneously fit SEDs and visibilities (Millan-Gabet et al., 2001; Akeson et al., 2002)). SEDs utilizing the standard disk model tend to underestimate the radius of the dust-free inner disk. Better fits to visibilities were obtained using simple geometric Gaussian or ring models. Although these models are not physically derived, the ring model may correspond to an optically thin inner gas disk

plus a hot, puffed-up wall of dust at the sublimation radius, as suggested by Natta et al. (2001) and Dullemond et al. (2001). Once the correct disk model is taken into account, the inner radius is consistent with the radius at which disk temperatures reach silicate grain sublimation temperatures, although a precise temperature can not be pinned down due to significant scatter in the data points (Monnier et al., 2005). Interestingly, this trend persists down to the lowest mass T Tauri stars observed, suggesting that the dust disk must truncate significantly further out than the gas disk, which is expected to extend inwards to about the stellar corotation radius (Eisner et al., 2005).

In addition to effecting this significant shift in our theoretical picture of inner disk structure, IR interferometry has suggested a few other trends. For example, as noted by Eisner et al. (2003) and Monnier and Millan-Gabet (2002), disks around the earliest-type Be stars in their samples (stars with $L \gtrsim 1000$ $L_\odot$) are actually best fit by the standard accretion disk model, consistent with an optically thick inner gas disk. This could signify a transition in the mode of accretion at about 1000 $L_\odot$. In addition, Akeson et al. (2005b) found that for some sources, models required significant gas emission from within the dust disk inner radius, a contribution not often considered in SED modeling. Finally, Akeson et al. (2005a) noted a possible anti-correlation between the ratio of accretion to stellar luminosity ($L_{\mathrm{acc}}/L_\star$) and the ratio of inner radius to dust sublimation radius. If the luminosity ratio is a proxy for age, this would suggest a clearing of the inner disk with time.

CO $v{=}1{\rightarrow}0$ emission is readily produced by the high temperatures and densities found in inner disks around young stars and thereby presents a complementary view of these regions. Although a few regions close to the central star are capable of producing molecular emission, the required temperatures, characteristic velocities, symmetric shapes and a noticeable correlation between emission line shape and inclination (Blake and Boogert, 2004) suggest an origin in the circumstellar disk (Najita et al., 2003). Because temperatures of at least a few 100 K are required to populate the $v = 1$ level, CO $v{=}1{\rightarrow}0$ emission is restricted to regions within ~ 1 AU, the same area probed by IR interferometry.

We present observations of CO $v{=}1{\rightarrow}0$ emission around a total of 15 T Tauri and Herbig Ae/Be stars which have also been observed via IR interferometry. We are prompted by the interferometric

studies to consider the inner extent of CO emission (which we will refer to as the CO inner radius), which can be determined by calculating the width of the CO emission lines and correcting for inclination effects. We investigate the relationship of CO inner radii with stellar luminosities and accretion rates, as well as to published dust inner radii, with the hope of obtaining further insight into the structure and processes of inner disks.

4.3   Observations and Reduction

Most of our spectra were obtained with NIRSPEC (McLean et al., 1998), a high-resolution (R$\sim$ 25000, FWHM$\sim$ 12.5 km s^{-1}) spectrometer on the Keck II telescope. The data were taken in the M-band in echelle mode with a 0.43″×24″ slit. Each source was observed in at least two grating settings, thereby encompassing wavelengths between $\sim$ 4.65 and 5.15 μm, with the exception of a hole between orders at $\sim$ 4.8–4.95 μm. This wavelength range covers the first two R-branch lines and the low/mid P-branch (J=1–12 and J=30–40) of the $v=1{\rightarrow}0$ CO rovibrational spectrum, as well as the H I Pf β and Hu ε transitions.

Our NIRSPEC observations are derived from several observing runs spanning the years 2001–2005. A summary of the observations is presented in Table 4.1. TW Hya's CO emission lines were not resolved with NIRSPEC and this source was therefore observed with Phoenix (Hinkle et al., 2003) on Gemini South. It was observed on 07 and 08 Apr. 2006 using the 0.35″×14″ slit. With its significantly higher resolution ($R \sim 60000$; FWHM ~ 5 km s^{-1}), Phoenix provided us with resolved emission lines from P(6) to P(9).

Objects were observed in nod pairs and then differenced to reduce thermal noise on the chip. Wavelengths were calibrated using atmospheric emission lines. Nearby standard stars were observed for additional atmospheric correction. A and B stars with few features in the near IR region were chosen, although H I lines were present and therefore fitted by Kurucz models before division. Standard stars were also utilized for flux calibration, using M-band fluxes estimated from 2MASS K-band photometry (Skrutskie et al., 2006) and spectral type. Wavelengths were also shifted to correct for Earth's motion.

4.4   Sources and Spectra

The dataset included in this article consists of the 20 T Tauri stars (TTSs) and Herbig Ae/Be (HAe/Be) stars listed in Table 4.1. These represent a small subset of our complete M-band survey, chosen because they showed CO $v=1\rightarrow0$ in emission and had measured masses, luminosities, and disk inclinations. Although our complete survey includes YSOs spanning a large range of evolutionary states, the sources with CO $v=1\rightarrow0$ emission tend to be class II TTSs and their HAe/Be counterparts (for example, those with Type I SEDs in Hillenbrand et al. (1992)). Less-evolved embedded sources often show CO $v=1\leftarrow0$ absorption instead, and more evolved sources are much less likely to show any CO emission or absorption signatures. This is consistent with the current belief that the CO emission arises from the surfaces of circumstellar disks; in less evolved sources, the disks are obscured by foreground material and in more evolved sources, the CO does not exist at high enough densities and temperatures to be visible.

We show two example spectra in Figure 2.1—one for T Tauri star DR Tau and one for HAe/Be star AB Aur. The most apparent feature is a set of $v=1\rightarrow0$ emission lines extending from R(2)– P(40). Other features include the prominent, wide HI Pf β and Hu ε lines, a dust plus photosphere continuum, and, for DR Tau, ^{13}CO $v=1\rightarrow0$ and CO $v=2\rightarrow1$ emission. Spectra line shapes may be nearly-Gaussian, double-peaked, flat-topped, or occasionally asymmetric (discussed in more detail in Section 4.5). Except for line widths and shapes, which we discuss in Section 4.5, most of the spectral features are not obviously correlated with stellar or disk parameters and are therefore not easy to predict. However, this may not be too surprising given the complex environment that gives rise to the emission; the spectrum depends on the radial and vertical temperature and density distributions of the disk gas and dust, the viewing geometry of the disk, and properties of the stellar photosphere and any foreground material.

4.5 Emission Line Structure

CO v=1→0 emission is believed to originate from the inner regions of Keplerian disks, because of the conditions required for its production (high densities and temperatures, and significant vertical gradients) and because line shapes are fairly symmetric and dependent on disk inclination (Najita et al., 2003; Blake and Boogert, 2004). With the assumption that the emission lines originate in a circumstellar disk, one can in principle correct for disk inclination and derive the inner extent of CO emission (hereafter the CO inner radius) from the line widths.

One needs to be cautious when determining the CO inner radius, however, because the line shape also depends on the gas and dust temperature and density profiles as well as the degree of non-Keplerian broadening. Ideally, analysis would be performed with a 2D disk model that generates both SEDs and emission lines. However, we focus in this article on a much simpler approach to approximately determine the CO inner radius. We begin by compiling emission line composites from the emission lines that are least contaminated by other CO lines or telluric features. Then, we utilize Gaussian fits to the composite lines and assume that the wings of the profile represent emission from the inner edge of the CO disk. Precisely defining the CO inner radius based on these fits is not entirely straightforward, and we describe our procedure in more detail in Section 4.5.2.

We begin this section by discussing the process of constructing the line composites. Then, we discuss the major emission line features seen in our sources. Finally, we discuss in detail our fitting methods and our estimation of the CO inner radius.

4.5.1 Constructing Line Composites

To investigate emission line shapes and widths, we created normalized, continuum-subtracted composite lines from our spectra. We used only P-branch lines to construct the composites, because R(0) and R(1) lie on top of the HI emission lines. When emission lines were present in both M-band orders, we created a composite for each order, to preserve any differences between low and high energy line shapes. One composite is constructed from emission lines up to P(18) and the other from emission lines P(30) and up. For some stars one of the orders was not observed or was lacking

CO emission, and in these cases only one composite emission line was created. For each composite, we only utilized emission lines that were easily identifiable above the continuum level, that had fairly complete velocity coverage after the removal of telluric contamination, and that were not too entangled with other emission lines (such as CO $v=2\rightarrow1$ or ^{13}CO). The P-coefficients of the lines used to construct each composite are listed in Table 4.2.

To construct composites, lines were isolated, continuum subtracted, and normalized to a height of 1. Then, each line was centered according to its wavelength in the HITRAN database (Rothman et al., 1992), wavelengths were converted to velocities, and lines were overlapped. Contamination from nearby lines was removed by eye. Finally, composite lines were constructed using linear interpolation, with a bin size set such that each bin contained approximately five data points. (An exception was made for TW Hya for which this criterion yielded insufficient points for a proper fit). Bin sizes ranged from 2–10 km s^{-1}.

4.5.2 Emission Line Features

The complete set of composite lines used in this study is shown in Figure 4.2. A variety of line shapes is apparent, including nearly Gaussian, double-peaked, flat-topped, and emission plus absorption. This is in general agreement with emission shapes expected from a Keplerian ring of hot gas, plus cooler foreground gas, for different disk geometries. A disk origin for the CO emission is also consistent with the observation that, for most sources, the P> 29 emission line composite is somewhat wider than the P< 19 composite. Due to radial temperature gradients and any resonance fluoresence, the high-P composite should have proportionally more flux coming from closer to the star, where Keplerian velocities are higher; this will tend to puff up the wings of the emission profile, making it appear broader.

Asymmetric lines are derived for AA Tau, DO Tau, HD 163296, VV Ser, and RY Tau. Asymmetry could either be the result of physical phenomena or the result of improper atmospheric correction, since atmospheric and object lines are offset due to Doppler shifts. For AA Tau, DO Tau, and HD 163296, velocity coverage is not complete and line features vary somewhat when atmospheric removal

criteria are varied. Therefore, we should be cautious about attributing these features to physical phenomena. On the other hand, VV Ser and RY Tau were both observed on several occasions and at a variety of Doppler shifts, and the asymmetry is a robust feature of their emission lines. Interestingly, for four out of the five stars, and for three stars observed by Najita et al. (2003), the blue peak is higher than the red peak. Absorption by infalling gas has been suggested as an explanation for this asymmetry (Najita et al., 2003), although we caution that we see no correlation between the presence of asymmetry and accretion rate and/or inclination.

4.5.3 Deriving Inner Radii

Our procedure for deriving CO inner radii was the following. Firstly, we fit each emission line with a simple mathematical model: either one or two Gaussians, depending on its shape, as plotted in Figure 4.2. For the two-Gaussian fits, there were often several minima, so we restricted the solutions to those with a wide positive plus narrower negative Gaussian. The negative Gaussian may represent a dip due to the double-peaked nature of inclined, ring-like emission, or it may represent absorption due to foreground emission. The FWHMs of the positive Gaussians are listed in Table 4.2. We also include in our analysis the FWHMs derived for several additional T Tauri stars by Najita et al. (2003) (see Tables 4.3 and 4.2).

It is important to carefully choose a reference point on the Gaussian curve to represent the CO inner radius. Previous researchers have generally used the velocity corresponding to half width at zero intensity (HWZI) as a convenient estimate (Brittain et al., 2005; Najita et al., 2003). However, non-Keplerian motion can also be important in widening emission lines, so the velocity at HWZI is better seen as a lower limit to the inner radius. Our own 2-layer disk models for TW Hya and GM Aur (Salyk et al., 2007) yielded inner radii of $0.2^{+0.4}_{-0.05}$ and $0.3^{+0.2}_{-0.15}$ AU, respectively, which correspond to approximately $1.5 \times$ HWHM and $2.2 \times$ HWHM. In contrast, the HWZI corresponds to roughly $2.5 \times$ HWHM for most stars in our sample. For our analysis, we utilize the velocity at $1.85 \times$ HWHM as a best estimate of the inner radius. (These velocities are indicated as solid lines in Figure 4.2). As a lower limit, we utilize $2.5 \times$ HWHM, corresponding approximately to the HWZI.

The upper limits to the inner radii in Salyk et al. (2007) are 0.6 AU for TW Hya and 0.5 AU for GM Aur; these correspond to velocities at 0.9 and 1.65×HWHM. As a conservative estimate of the upper limit, therefore, we utilize 0.9×HWHM. These radii are smaller than, and therefore consistent with, the outer emission radii estimated by Najita et al. (2003).

As mentioned in Section 4.5.1, high-P and low-P line composites differ slightly in character and width. Whenever possible, we utilized the high-P line composites to estimate the inner radii used in our analysis, because they are less likely to be contaminated by telluric or foreground CO. A clear demonstration of this choice can be seen with DO Tau, for which the low-P composite appears narrow and oddly asymmetric. These features are apparently due to telluric contamination, or to a combination of telluric and foreground absorption. The high-P composite shows no evidence for such contamination; it is symmetric and much wider. Whenever there was only a low-P composite, however, we utilized this composite instead.

We used the stellar and disk parameters listed in Table 4.3 to convert velocities to inner radii, with the assumption that the emission comes from a Keplerian disk. Note that we will generally assume that the CO inner radius is equivalent to the inner extent of CO in the disk, although in a well-mixed region of the disk in which there is no significant vertical temperature gradient, CO may exist yet not appear in emission. To determine error bars, we added (in quadrature) uncertainties based on the limits discussed above and uncertainties in system inclination. When inclinations were published without error bars, we used a default error of ±10°. Calculated CO inner radii are shown in Table 4.2.

4.6 Results

For low-mass/low-luminosity T Tauri stars (stars with luminosities below $\approx 5L_\odot$), the CO inner radius is consistent with the corotation radius. For higher-mass stars, the two radii are not consistent.

For a sample of five T Tauri stars observed by Najita et al. (2003), CO inner radii were found to be in the range ~ 0.5–1 times the corotation radius. The corotation radius is defined as the radius

at which the disk's Keplerian angular velocity is the same as that at the stellar surface, and is given by:

$$R_c = \frac{GM_\star R_\star^2 \sin^2(i)}{(\mathrm{v}\sin(i))^2}. \tag{4.1}$$

This radius is in turn approximately equal to the magnetic truncation radius, within which disk material is expected to have been cleared by magnetospheric accretion (Shu et al., 1994). With this previous result in mind, we have compared CO inner radii and corotation radii in Figure 4.4 for the stars in our sample and the stars observed by Najita et al. (2003) (with the exception of three stars for which no velocity data were available).

For convenience, we have assumed that $i_\star = i_{\mathrm{disk}}$, although the two need not be exactly the same, and in fact are offset by about 6° in our own solar system. In Figure 4.4, symbol sizes are proportional to stellar mass, and we differentiate between TTSs and HAe/Be stars. The solid line is a 1:1 corresondence between the two parameters. It is apparent that many of the lower-mass TTSs have CO inner radii similar to or some fraction of their corotation radius. However, for the higher-mass TTSs and all HAe/Be stars, the CO inner radius is quite a bit larger than the corotation radius, so that CO inner radius is not set by magnetic interactions between the star and disk.

For most low–medium mass stars in our sample, CO inner radii are consistent with dust sublimation radii.

As a result of interferometric observations of inner disks, it has become apparent that dust inner radii are set by sublimation, rather than magnetospheric effects such that $R_{\mathrm{dust}} \propto L_\star^{1/2}$. A similar trend could be expected for CO inner radii because of an important connection between CO and dust—dust shielding is required for the protection of molecular CO against dissociation by stellar UV (van Dishoeck and Black, 1988). We therefore plot CO inner radius as a function of stellar luminosity in Figure 4.5 and overplot theoretical curves for the dust sublimation radius as a function of luminosity. The curves are derived from the formula for blackbody grains in an optically thin disk:

$$T_{\mathrm{sub}} = \left(\frac{L_\star}{16\sigma\pi r_{\mathrm{sub}}^2}\right)^{1/4}. \tag{4.2}$$

This formula neglects grain properties and effects such as disk backscatter, but differs from the results of more in-depth analyses (e.g., Monnier and Millan-Gabet, 2002) by a constant of order unity. (A more complete discussion of various physical models and their differences can be found in Akeson et al., 2005a). We plot curves for three different grain sublimation temperatures—1000, 1500 and 2000 K. Because luminosities are generally published without error estimates, we adopt an error bar of 10%, which is consistent with the errors found by Monnier et al. (2005), which range between a few % and $\sim 50\%$. Up to luminosities of $\sim 11\, L_\star$ CO inner radii for most stars are consistent with the dust sublimation radius.

If inner radii were instead set by the stellar corotation radius (R_c), the slope of radius versus luminosity would be shallower. For example, an empirical fit to our dataset yields $R_c = 0.0001(L_\star/L_\odot) + 0.045$ AU ≈ 0.045 AU. We include R_c and $0.5R_c$ in Figure 4.5 for comparison. Note that at low luminosities, sublimation radii and corotation radii are similar, so it is not possible to decide the physical cause of the CO disk truncation. However, at higher luminosities, it is clear that radii are not consistent with being set by magnetospheric accretion.

CO inner radii are correlated with measured dust inner radii. However, for lower mass stars the tendency is for $\mathbf{R_{CO} < R_{dust}}$, while for higher mass stars, it's more common that $\mathbf{R_{CO} > R_{dust}}$.

Because we expect CO inner radii to be determined by the availability of dust to act as a UV shield, we plot CO inner radii against dust inner radii (hereafter referred to as $R_{\rm dust}$) in Figure 4.6. Values and error bars for dust inner radii are taken from the references found in Table 4.3. Error bars for the CO inner radii are the same as in Figure 4.5. The dashed line is a 1:1 correspondence between the two radii.

We were surprised to find a number of low–mid-mass stars for which $R_{\rm CO} < R_{\rm dust}$. We suggest two possibilities for the existence of such sources. The first possibility is that the timescale for mass replenishment via accretion could be shorter than that of CO removal by UV dissociation. In this scenario, the CO inner radius would be set at a point inside the dust inner radius where the radiation field was strong enough for mass removal by dissociation to dominate. This effect

would also conveniently explain why we find $R_{\mathrm{CO}} < R_{\mathrm{dust}}$ for only lower mass stars, as it would be seen preferentially around stars with low UV luminosities. To obtain a rough measure of the two timescales, we consider a 4000 K, $2R_\odot$ star and compare the dissociation lifetime at 0.05 AU with the time required to fill a gap between 0.05 AU and 0.1 AU by accretion. Utilizing the CO dissociation rates found in van Dishoeck et al. (2008) and assuming no dust shielding, we derive a lifetime for molecular CO at 0.05 AU of ~ 5 yr. (For comparison, the lifetime for CO sitting 0.05 AU from a 10000 K blackbody is 0.05 s.) On the other hand, with an accretion rate of $10^{-7}\,M_\odot/\mathrm{yr}$, a gap between 0.05 and 0.1 AU can be filled to a surface density of $10^{-4}\,\mathrm{g\,cm^{-2}}$ in only 0.01 yr. However, this is not the whole story, as UV fluxes are greatly enhanced for accreting protostars. For example, at 0.1 μm, the wavelength primarily responsible for the dissociation of CO (van Dishoeck and Black, 1988), Bergin et al. (2003) estimate that a typical TTS has a flux of $\sim 5 \times 10^{-4}\,\mathrm{erg\,cm^{-2}s^{-1}A^{-1}}$ at 100 AU—an enhancement of nearly 8 orders of magnitude over the reference 4000 K blackbody considered above. With UV fluxes this high, destruction of CO by dissociation is by far the dominant process, and CO inner radii would not be expected to lie within dust radii. The balance of processes for any individual T Tauri star could potentially lie somewhere between these two cases and therefore mass replenishment by CO may be the cause of small CO inner radii for some sources. However, given the large number of such sources, it does not seem the most likely explanation.

The large number of sources with $R_{\mathrm{CO}} < R_{\mathrm{dust}}$ may alternatively be explained by the presence of non-Keplerian motion in the inner disk (turbulence, inflow, or outflow). As discussed in Salyk et al. (2007), the degree of turbulence can be a crucial parameter when fitting emission lines with disk models if the emitting disks have low inclinations. We have assumed only low levels ($v_{\mathrm{th}} = 0.05\,v_{\mathrm{Kep}}$) of turbulent motion when estimating CO inner radii and thus if significant non-Keplerian motion exists, we would falsely attribute it to faster Keplerian motion at smaller radii. However, this is a testable hypothesis, since the percent discrepancy due to thermal motion would be dependent on disk inclination. If we assume $v_{\mathrm{th}} = \alpha v_{\mathrm{Kep}}$, and that v_{th} is isotropic, then the percent discrepancy in radius is given by $\alpha/\sin i$, where α is likely a few percent. If we assume $R_{\mathrm{actual}} \sim R_{\mathrm{dust}}$ then the percent discrepancy in radius should be given by $(R_{\mathrm{dust}} - R_{\mathrm{obs}})/R_{\mathrm{obs}}$. Our dataset, however,

demonstrates no correlation between radius discrepancy and $\alpha/\sin i$. Some other form of non-Keplerian motion could also cause the discrepancy although a key signature of inflow and outflow—line asymmetry—is not prevalent amongst the CO lines in our dataset. This is especially true of the subset for which $R_{\mathrm{CO}} < R_{\mathrm{dust}}$, amongst which only one star (RY Tau) displays line asymmetry.

In short, underestimation of CO inner radii seems a likely explanation for why measured CO inner radii appear to lie inside dust inner radii, although we have not found a satisfying physical explanation for this effect.

We discuss a number of high-mass sources for which $R_{\mathrm{dust}} < R_{\mathrm{CO}}$ in our next point.

For HAe/Be stars with $L \gtrsim 11\,L_{\odot}$, CO inner radii are significantly larger than dust sublimation radii and measured dust inner radii.

In order to visualize all of the various theoretical and measured radii, we have included Figure 4.7. In this figure, we have plotted theoretical dust sublimation radii, corotation radii calculated via Equation 4.1 and measured dust and CO inner radii for each star. Stars are organized in order of luminosity, with higher luminosity sources towards the bottom.

With the exception of HD 144432, for all sources with $L \gtrsim 11\,L_{\odot}$, measured dust inner radii appear consistent with theoretical dust sublimation radii. However, CO inner radii are much larger than sublimation radii, with the ratio $R_{\mathrm{CO}}/R_{\mathrm{sub}}$ ranging from 2–13. This could be indicative of differences in disk geometry between T Tauri/low-mass Herbig Ae stars and higher-mass Herbig Ae/Be stars. Indeed, inteferometric observations have suggested a boundary at $\sim 1000\,L_{\odot}$ between disks with optically thin inner regions and hot inner rims, which tend to have larger inner radii, and disks with optically thick inner regions, which tend to have smaller inner radii (Akeson et al., 2005b). Additionally, results from Hα spectropolarimetry have suggested different inner disk geometries for T Tauri/Herbig Ae stars as opposed to Herbig Be stars (Vink et al., 2002). However, these results both suggest a partition at a higher luminosity ($\sim 1000\,L_{\odot}$) than we observe in our dataset. In addition, they suggest that higher mass sources have something closer to the 'classical' thin disk, with an optically thick inner disk and hence a *smaller* sublimation radius. Therefore, this particular geometric effect does not explain our results.

Another geometric effect that could cause an increase in the observed CO inner radius is self-shadowing. We consider the self-shadowed disk model from Dullemond et al. (2001), for which stellar parameters are quite similar to the HAe stars in our sample. In this model, the disk region within $\sim 1\,\mathrm{AU}$ has virtually no vertical temperature gradient, so that it is unlikely to show molecular emission, even if molecules are present. Between 1–2 AU vertical temperature gradients emerge, and disk surface temperatures approach those capable of inducing vibrational transitions. This distance corresponds well with the CO inner radii of HAe stars in our sample. However, if this effect is to explain our results, we should see a correlation between SED type and $R_{\mathrm{CO}} - R_{\mathrm{sub}}$, but this appears not to be the case. Six of our sample stars have had their SEDs classified as I (flared) or II (self-shadowed) by Meeus et al. (2001) and Acke et al. (2004). Of these six, one (AB Aur) has been classified as type I, although it has a CO inner radius slightly larger than the dust sublimation radius. The remaining five (HD 141569, HD 144432, HD 163296, MWC 480, and VV Ser) have all been classified as type II and most have unusually large CO inner radii, although one (MWC 480) actually has a CO inner radius well inside the sublimation radius. Thus, there is no conclusive evidence that self-shadowing effects can explain our results, although with the small number of sources considered, it cannot be ruled out.

Another possibility one might propose to explain why $R_{\mathrm{CO}} > R_{\mathrm{sub}}$ for high-luminosity sources is that their high UV flux penetrates a significant distance into the dust disk to dissociate CO. To test this hypothesis, we must determine whether the penetration depth of UV radiation is similar to $R_{CO} - R_{dust}$. We define the penetration depth as the depth at which the dissociation rate equals the rate of replenishment via accretion. Considering a ring from 0.5 to 1 AU, which is the typical ring between R_{CO} and R_{sub} for the HAe stars in our sample, an accretion rate of $10^{-7}\,M_{\odot}/\mathrm{yr}$ and a surface density of dust $\Sigma = 22 \times (r/AU)^{-1.5}\,\mathrm{g\ cm}^{-2}$, the replenishment timescale is $\sim 80000\,\mathrm{yr}$. According to the dissociation rates given in van Dishoeck et al. (2008) for a 10000 K blackbody, 80000 years is the dissociation timescale at $\tau \sim 8$. This optical depth is reached in a very short distance along the disk midplane, but we are concerned with the existence of CO in a disk atmosphere, where densities are significantly lower. In this case, the amount of extinction for a light ray depends quite

sensitively on the vertical height of the CO emitting region. With a simple disk density prescription, as described in Ruden (1999), and with opacity as defined in Eisner et al. (2006), we estimate that optical depths of ~ 8 are equivalent with $R_{CO} = 1$ and $R_{dust} = 0.5$ if $z/r \sim 0.5$, where z is the height of the emitting layer. This is quite high and implies CO densities of order 10^{-7} g cm^{-2}—orders of magnitude lower than that found by Salyk et al. (2007). In addition, given this setup, one would expect large $R_{CO} - R_{dust}$ to correspond to low densities and, hence, lower line fluxes. However, we do not see evidence for such a correlation. Therefore, UV penetration into the dust disk is not a likely explanation for the large CO inner radii.

In short, the preponderance of high-mass HAe/Be stars for which $R_{CO} > R_{sub}$ and $R_{CO} > R_{sub}$ suggests a transition in disk geometry at $\sim 11\, L_\odot$, although the exact nature of the transition is not yet understood.

Amongst the T Tauri stars, there are three notable outliers for which $R_{CO} \gg R_{sub}$: TW Hya, GM Aur and DR Tau.

TW Hya, GM Aur, and DR Tau have inner radii that lie significantly above the curves for dust sublimation or corotation. It is interesting to note that two of the three sources, TW Hya and GM Aur, are prototypical examples of transitional disks—disks with large inner regions of low opacity within an otherwise optically thick disk, perhaps due to the presence of a planet (Rice et al., 2003; Calvet et al., 2002). For such disks, one might expect the CO inner radius to correspond not with the dust sublimation radius, but instead with the edge of the optically thick outer disk. However, this does not appear to be the case. Although the inner disks of transitional objects are relatively free of dust, they are not entirely so and in fact dust was detected at radii of 0.06 AU (Eisner et al., 2006) and 0.221 AU (Akeson et al., 2005b) for TW Hya and GM Aur, respectively. According to Figures 4.6 and 4.7, the CO inner radii lie just outside of these dust inner radii (see also Salyk et al. (2007)). Since the inner dust disks are optically thin, R_{CO} must be slightly greater than R_{dust} to provide significant UV shielding. Interestingly, the dust inner radii themselves are larger than the expected dust sublimation or corotation radii by factors of $\sim$ 3–5, suggesting that perhaps there has been dynamical clearing of the inner disk.

DR Tau is another notable outlier according to Figures 4.5 and 4.6. We first note that the lower error bar is quite large due to large uncertainties in the system inclination, and that may be the explanation for DR Tau's apparent outlier status. However, there is another physical reason why DR Tau may appear to be an outlier—accretion rates for DR Tau are at least an order of magnitude above those of typical T Tauri stars (Hessman and Guenther, 1997). In Figure 4.5, we plotted stellar luminosity as the abscissa, but the energy from accretion luminosity is also available for heating of the disk, and hence for sublimating grains. For most stars in our sample, the stellar luminosity dominates. However, for two sources, DR Tau and HL Tau, the accretion luminosity may be a magnitude or two larger. If we use the relationship of Hartmann et al. (1998) to estimate accretion luminosity,

$$L_{\mathrm{acc}} = 0.8\, G \dot{M}_{\mathrm{acc}} M_\star / R_\star, \tag{4.3}$$

and mass accretion rates from Johns-Krull and Gafford (2002), we find that DR Tau's accretion luminosity is $\sim 32\, L_\odot$ (using an average of the accretion rates in Johns-Krull and Gafford (2002)). If placed in Figure 4.5 according to this enhanced luminosity, its CO inner radius becomes consistent with the dust sublimation curve. It is interesting to note that HL Tau, with a $L_{\mathrm{acc}} : L_\star$ ratio of about 11, does not appear to be an outlier, and by using the total luminosity, we find that CO inner radius lies somewhat inside of the $T = 2000\,\mathrm{K}$ sublimation radius. For both sources, it is important to keep in mind that these simple analytical calculations are not taking into account the time variability of T Tauri phenomena. Indeed, DR Tau is known for displaying a high degree of veiling, which is variable on both short and long timescales (Hessman and Guenther, 1997), and HL Tau has an active outflow and shows evidence for periodic large outbursts (Close et al., 1997).

Our results do not indicate an anti-correlation between the ratio of CO inner radius to predicted sublimation radius and the ratio of accretion luminosity to total luminosity.

Based on dust inner radii measurements for 8 T Tauri stars, Akeson et al. (2005a) noted an apparent anti-correlation between the ratio of measured dust inner radius to theoretical sublimation radius and the ratio of accretion to stellar luminosity. This makes intuitive sense; as a star evolves, accretion rates tend to decrease and inner disks should be cleared by some combination of accretion,

photo-evaporation, and planetesimal formation. If the dust inner radius increases with age, the CO inner radius should also increase, and this could potentially explain some of the scatter in Figure 4.5.

With this physical motivation in mind, we plot the ratio of $R_{\mathrm{CO}}/R_{\mathrm{sub}}$ against the ratio $L_{acc}/L_{\star}$ in Figure 4.8. To provide a consistent estimate of accretion luminosity, we use Equation 4.3. We calculate the sublimation radius using Equation 4.2, with $T_{\mathrm{sub}} = 1500\ K$. For DR Tau and HL Tau, we use L_{acc} in place of $L_{\star}$ when calculating the sublimation radius.

It is apparent that TW Hya and GM Aur have significantly higher radius ratios than the other TTSs in our sample—a point easily inferred from Figure 4.5. The presence of these two outliers gives a slight downward trend to the dataset, but, a linear fit to the radius ratio against the luminosity ratio yields a just slightly negative slope, with an associated p-value of 95%. Therefore, the dataset is consistent with the two ratios being uncorrelated. This raises some interesting ideas. One possibility for a lack of correlation may be that the luminosity ratio is not a predictive age indicator—intrinsic population heterogeneity could hide any existing age trends. Another possibility is that GM Aur and TW Hya are simply a different breed—i.e., perhaps the formation of inner disk gaps is not a typical evolutionary stage but may occur or not, depending on the particulars of the young stellar system.

4.7 Conclusion

We have detected CO rovibrational emission lines from a variety of young stars with disks, including classical T Tauri stars, transitional objects, and HAe/Be stars encompassing a wide range of luminosities, accretion rates, and disk characteristics. An analysis of line shapes shows that they are consistent with originating from an inner disk atmosphere, although line asymmetries in some sources suggest additional emission from regions of gas inflow or outflow. If asymmetries are due to inflow or outflow, this would imply accretion is occurring well outside the corotation radius.

An analysis of line widths suggests that the inner extent of emission in disks is well correlated with dust inner radii and as well as dust sublimation radii. This result is consistent with the models

suggested by IR interferometry, in which the inner gas disk is optically thin. Thus CO rovibrational emission provides a convenient validation of the assumptions made in interferometric analyses and provides an extension to the stellar population available for testing theories of inner disk structure.

Deviations from the $r_{CO} = r_{sub}$ trend also tell an interesting story. A number of T Tauri stars have unusually small CO inner radii, compared to the dust inner radius, even though the CO must be exposed to a significant amount of dissociating UV radiation. If UV excess is small and accretion rates are high, replenishment rates could potentially outdo dissociation rates, but given typical UV excesses for T Tauri stars, this does not seem likely. Another possibility is that non-Keplerian motion is broadening the line shapes, and we are simply underestimating the inner radius by assuming Keplerian motion only.

Transitional objects have unusually large CO inner radii as well. This is primarily due to the fact the dust inner radii are themselves quite large compared to the dust sublimation radius, possibly due to dynamical clearing or grain growth in the inner disk. However, CO inner radii are also significantly larger than dust inner radii, so perhaps the UV radiation is able to dissociate CO some distance into these relatively thin dust disks.

High mass HAe and the single HBe star in our sample also demonstrate unusually large CO inner radii, compared to both the dust inner radii and sublimation radii, which are themselves quite similar. This interesting discrepancy appears only for those stars with $L \gtrsim 11\,L_\odot$, which does not, to our knowledge, correspond to any known transitions in disk or stellar structure. We have considered a few ways in which disk geometry might cause enlarged CO inner radii; although none seem to securely explain our results, one possibility may be a transition between self-shadowing and flared disks.

We have also investigated the relationship between R_{CO}/R_{sub} and $L_{acc}/L_\star$, with the theory that radii may increase with age (and hence decrease with accretion rate) because of inner disk clearing. We note that the transitional disks, TW Hya and GM Aur, have higher R_{CO}/R_{sub} than all other sources, and also a relatively low $L_{acc}/L_\star$. However, there is no general trend between the two variables. This may simply be because accretion luminosity is not an exact proxy for age, or it

may indicate that TW Hya and GM Aur are unique and do not represent a common phase of disk evolution.
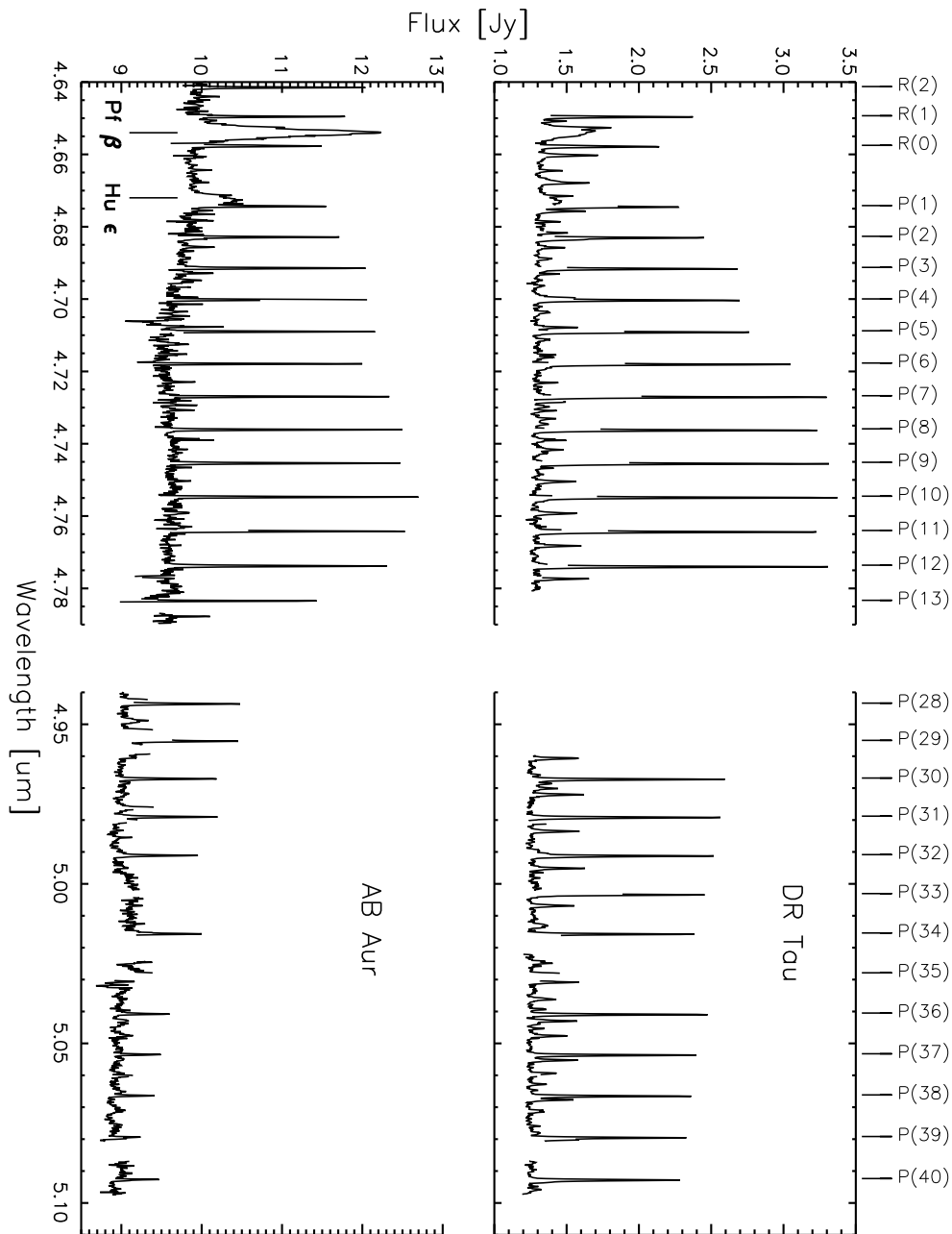
Figure 4.1: NIRSPEC spectra of T Tauri star DR Tau and Herbig Ae star AB Aur. CO v=1→0 transitions are labeled above, and H Pfβ and Huε transitions are labeled below. CO v=2→1 and ^{13}CO transitions are also visible in the spectrum of DR Tau.
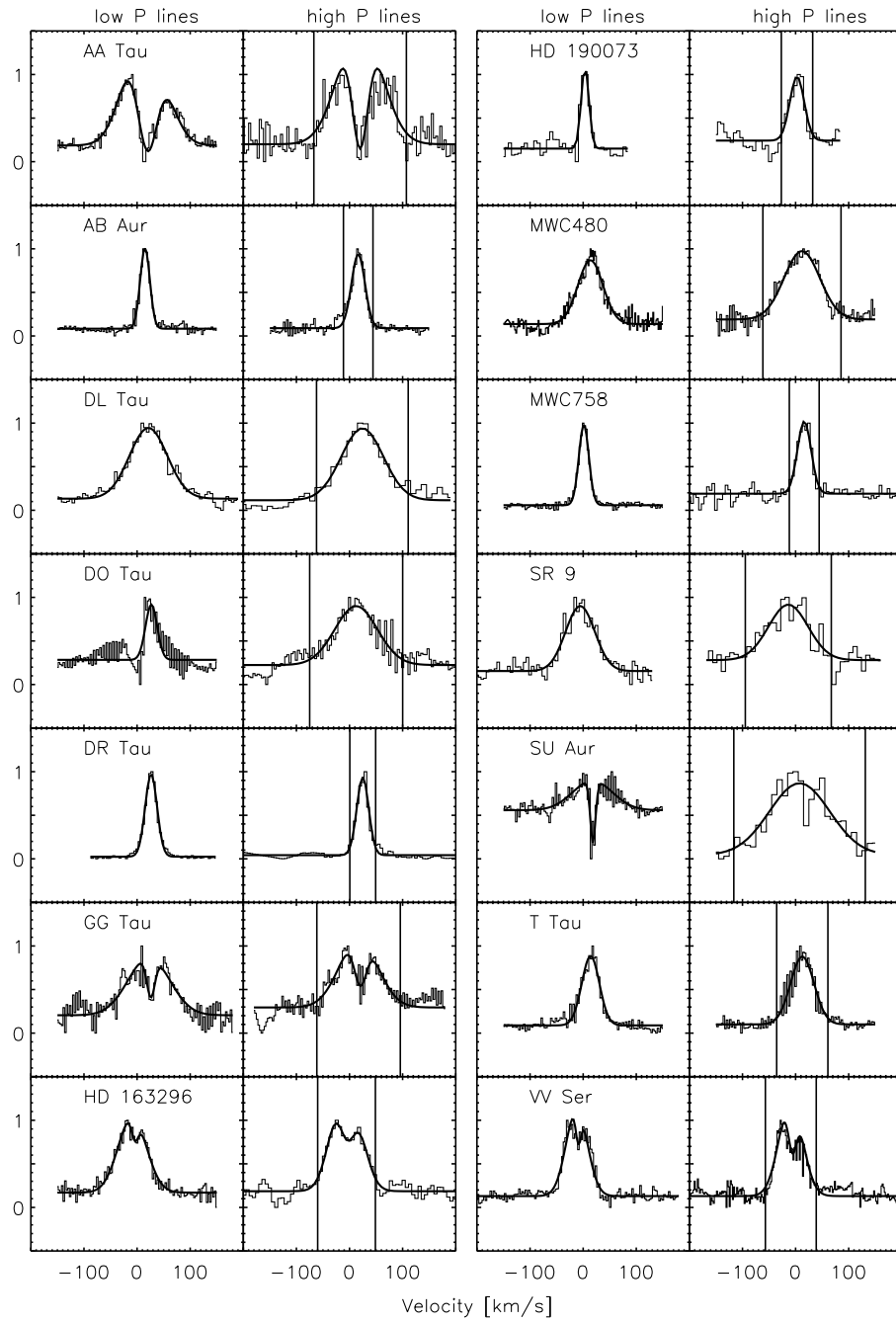
Figure 4.2: Composite emission lines, with one- or two-Gaussian fits. Vertical lines mark the velocity taken to represent the CO inner radius.
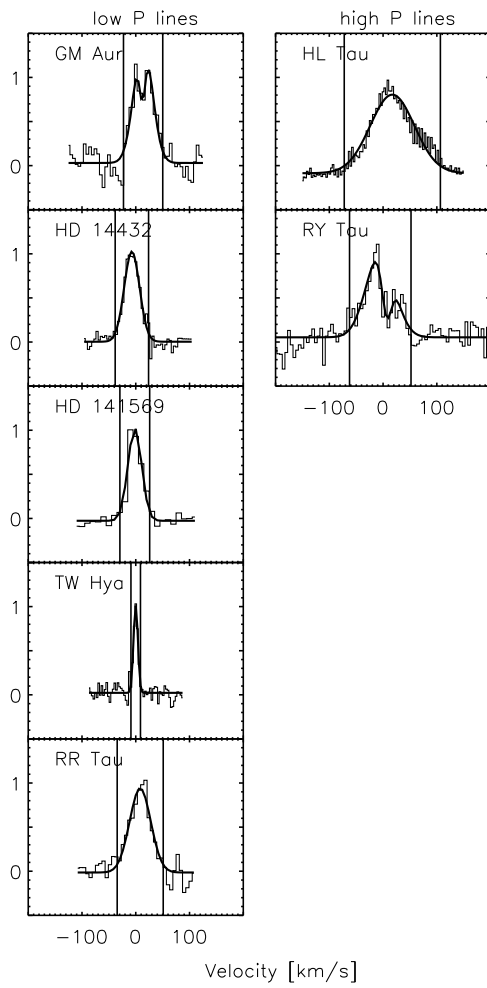
Figure 4.3: Composite emission lines for sources in which only one of the M-band orders was observed with CO $v=1 \rightarrow 0$ emission.

Figure 4.4: CO inner radius against corotation radius. T Tauri stars are represented as diamonds and HAe/Be stars as squares. The size of the symbol is proportional to the stellar mass. The solid line shows a 1:1 correspondence.
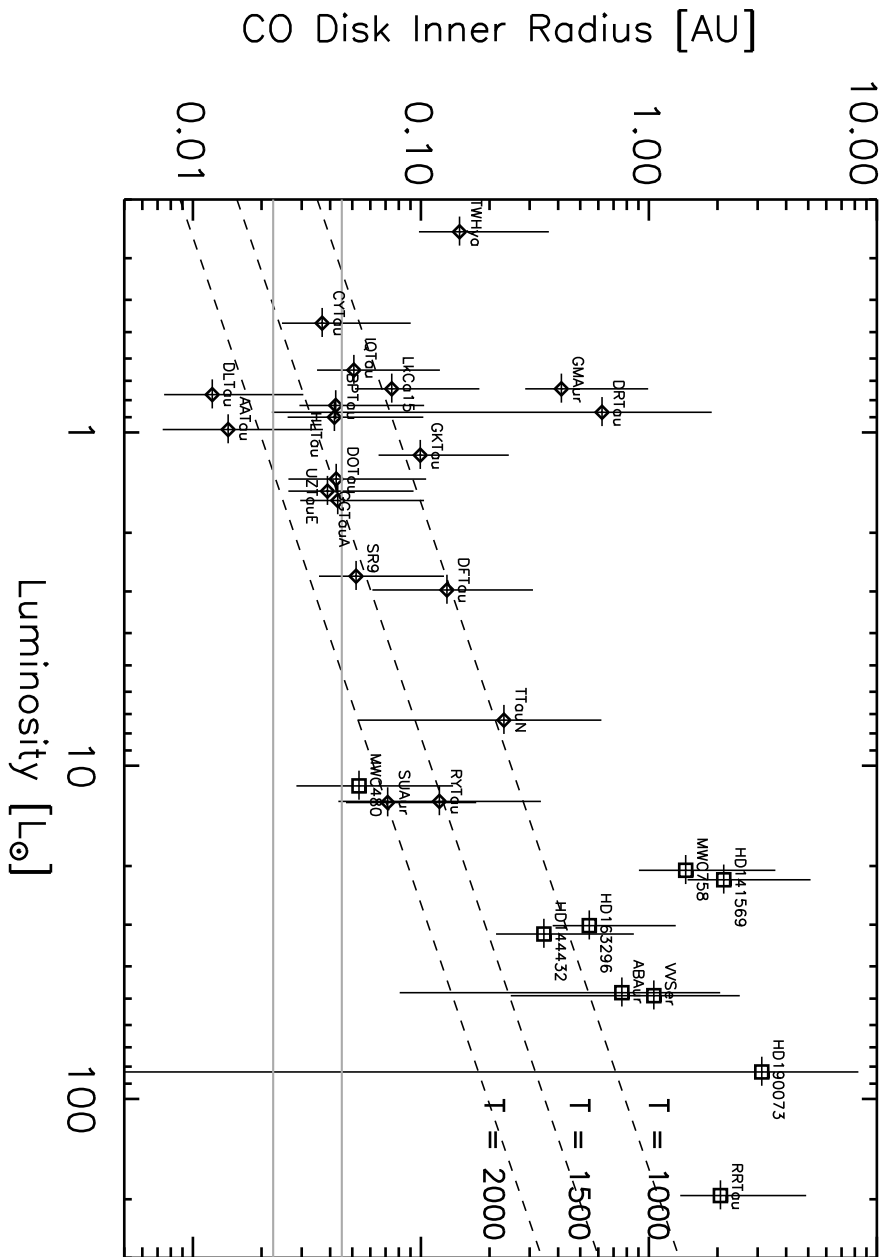
Figure 4.5: CO inner radius against luminosity. Diamonds are T Tauri stars and squares are HAe/Be stars. Dashed lines show theoretical curves for dust sublimation radius as a function of luminosity. Gray lines represent estimates of 0.5 and 1 corotation radii, based on an empirical fit to our dataset.
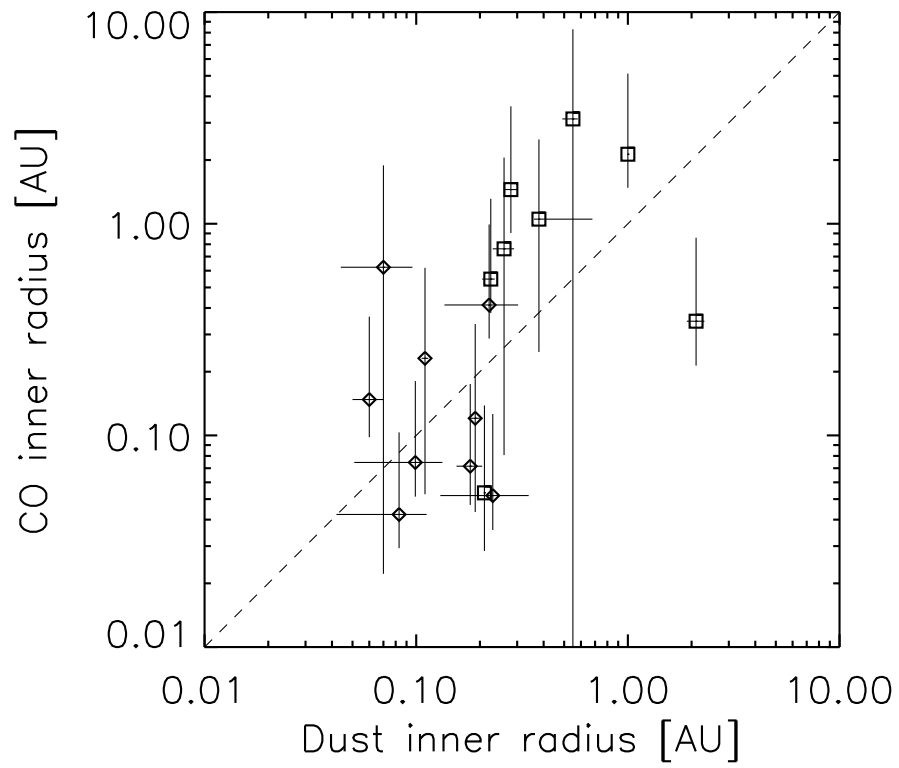
Figure 4.6: CO inner radius against dust inner radius. Diamonds are T Tauri stars and squares are HAe/Be stars. Dust inner radii are derived from IR interferometry results. A dashed line shows a 1:1 correspondence.
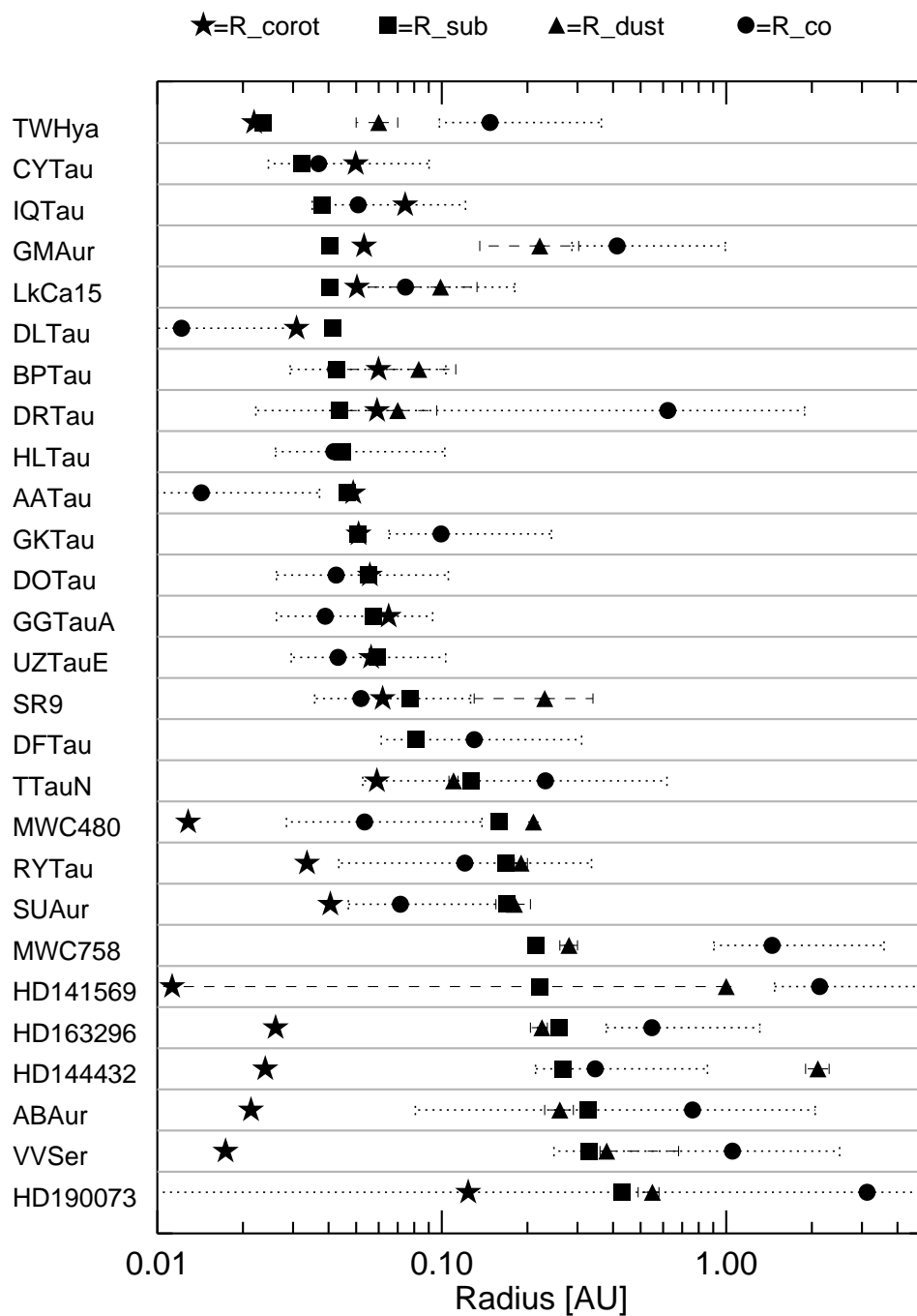
Figure 4.7: Relationships between all relevant disk radii: the disk corotation radius, the dust sublimation radius (with $T = 1500$ K), the dust inner radius (from interferometry, see Table 4.3) and the CO inner radius.Error bars for dust and CO inner radii are shown as dotted and dashed lines, respectively. Stars are arranged from top to bottom in order of luminosity.
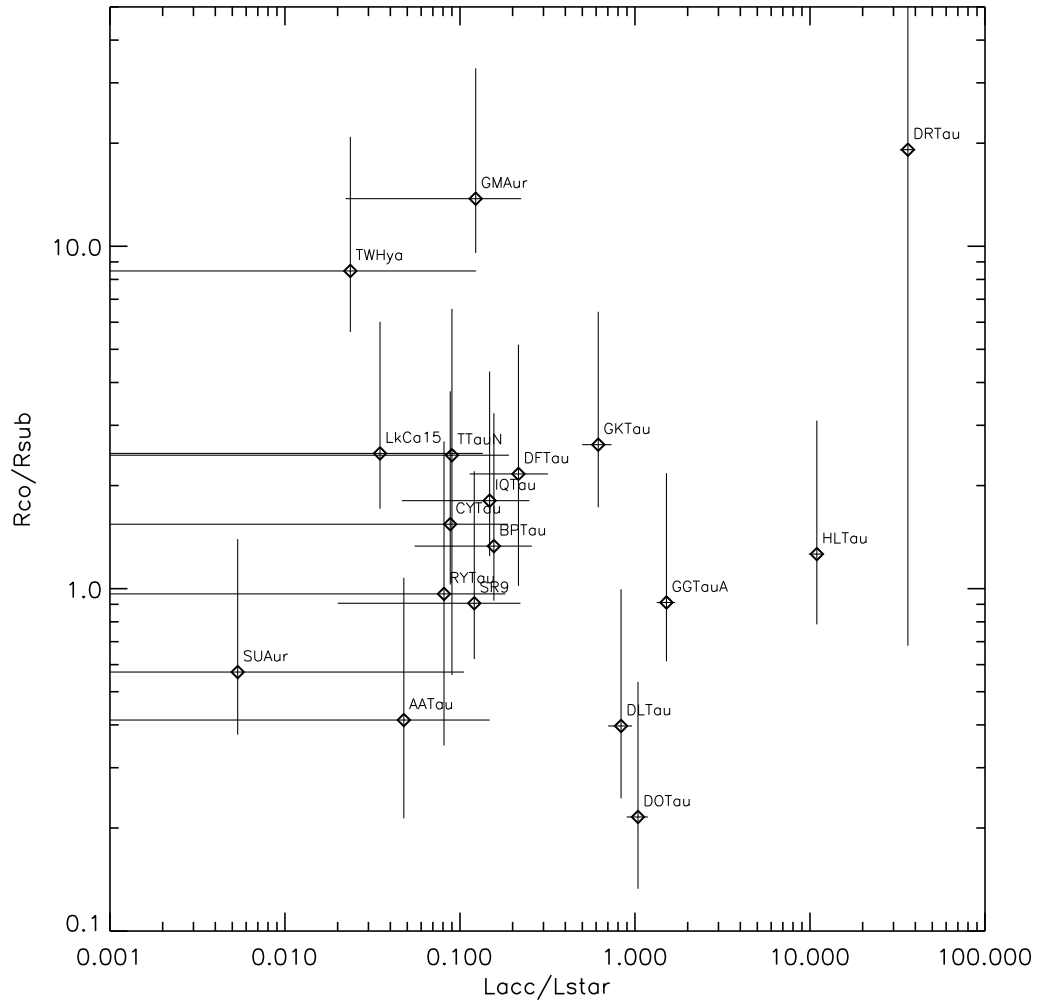
Figure 4.8: $R_{\mathrm{CO}}/R_{\mathrm{sub}}$ against $L_{\mathrm{acc}}/L_{\star}$. Diamonds are T Tauri stars and squares are HAe/Be stars.

Table 4.1: Summary of Observations

Star	Dates (mth/yr)	^{12}CO $1 \rightarrow 0$	$2 \rightarrow 1$	^{13}CO $1 \rightarrow 0$
AA Tau	11/03,12/04	✓	$\cdots$	$\cdots$
AB Aur	1/01,8/01,1/02,12/02	✓	$\cdots$	✓
DL Tau	11/03	✓	✓	$\cdots$
DO Tau	12/05	✓	✓	✓
DR Tau	12/02,12/05	✓	✓	✓
GG Tau A	1/02,12/02,1/02	✓	$\cdots$	$\cdots$
GM Aur	12/04	✓	$\cdots$	$\cdots$
HD 141569	4/02	✓	✓	✓
HD 144432	7/02,4/05	✓	$\cdots$	$\cdots$
HD 163296	8/01,4/02,7/02	✓	$\cdots$	$\cdots$
HD 190073	7/02,9/05	✓	$\cdots$	$\cdots$
HL Tau	10/01,12/02	✓	✓	$\cdots$
MWC 480	1/01,8/01,1/02,12/02	✓	$\cdots$	$\cdots$
MWC 758	4/01,12/02	✓	$\cdots$	$\cdots$
RR Tau	12/02, 12/05	✓	✓	$\cdots$
RY Tau	12/02	✓	$\cdots$	$\cdots$
SR 9	7/04	✓	$\cdots$	$\cdots$
SU Aur	12/02,11/03	✓	$\cdots$	$\cdots$
T Tau N	1/02,12/02,12/04	✓	$\cdots$	$\cdots$
TW Hya	1/01,4/02,12/02 12/04,4/05,12/05,5/06[a]	✓	$\cdots$	$\cdots$
VV Ser	8/01,7/03,7/04	✓	$\cdots$	$\cdots$

[a]observed with Phoenix

Table 4.2: Line Widths (FWHM)

Star	low J [km s^{-1}]	P coefficients	highJ [km s^{-1}]	P coefficients	R$_{in}$ [AU]
AA Tau	84	1-12	94	30-32, 36-40	$0.01^{+0.02}_{-0.01}$
AB Aur	22	1-12,14-15	30	26-32, 24, 36-40	$0.73^{+0.92}_{-0.70}$
DL Tau	84	2-6	93	30-32	$0.01^{+0.01}_{-0.01}$
DO Tau	26	1-12	95	30-33,36-40	$0.04^{+0.05}_{-0.02}$
DR Tau	26	1-12	26	30-34,36-40	$0.59^{+0.91}_{-0.60}$
GG Tau A	92	1-12	85	30-34,36-40	$0.04^{+0.04}_{-0.02}$
GM Aur	40	9-12,14	$\cdots$	$\cdots$	$0.41^{+0.42}_{-0.17}$
HD 141569	30	3-6	$\cdots$	$\cdots$	$2.05^{+2.12}_{-0.88}$
HD 144432	34	1-12	$\cdots$	$\cdots$	$1.07^{+1.15}_{-0.57}$
HD 163296	63	2-12,15	55	27-28,30-32,37	$0.54^{+0.56}_{-0.23}$
HD 190073	17	2-3,5-6,8-12	32	30-32,34,36-38	$3.03^{+3.68}_{-3.27}$
HL Tau	$\cdots$	1-8	97	27,30-34,36-40	$0.04^{+0.04}_{-0.02}$
MWC 480	56	2-4,6-12	80	26-32,36-38,40	$0.05^{+0.06}_{-0.03}$
MWC 758	22	1-12	30	30-33,36-38	$1.4^{+1.5}_{-0.73}$
RR Tau	46	8-12	$\cdots$	$\cdots$	$2.1^{+2.8}_{-0.7}$
RY Tau	$\cdots$	$\cdots$	62	30-32,34,36,38	$0.12^{+0.16}_{-0.09}$
SR 9	65	4,6,8-12	88	30-32,37	$0.05^{+0.05}_{-0.02}$
SU Aur	88	2-4,6-11	134	30-32	$0.07^{+0.08}_{-0.04}$
T Tau N	39	2-15,17	52	30-34,36-41,43	$0.23^{+0.28}_{-0.20}$
TW Hya	10	6-9	$\cdots$	$\cdots$	$0.14^{+0.15}_{-0.07}$
VV Ser	47	6-12	52	27-28,30-42	$1.04^{+1.07}_{-0.88}$

Table 4.3.   Stellar Parameters

Star	Type[i]	$M_\star$ [$M_\odot$]	$R_\star$ [$R_\odot$]	$L_\star$ [$L_\odot$]	i [°]	R_{dust} [AU]	$\dot{M}$ [$10^{-8}\,M_\odot$/yr]	v sin(i) [km s^{-1}]	refs
AA Tau	T	0.67	2.5	0.98	25 ± 7	$\cdots$	0.71	11	10,11,26,28
AB Aur	HA	2.4	2.5	48	28^{+10}_{-18}	0.26 ± 0.01	$\cdots$	80	9,38,38
DL Tau	T	0.56	2	0.77	25 ± 5	$\cdots$	9.3	16	10,14,26,28
DO Tau	T	0.72	1.78	1.38	45	$\cdots$	14.42	11.1	10,14,22,27
DR Tau	T	0.74	1.9	2.5	40 ± 30	0.07 ± 0.026	329.2	10[c]	7, 14,26,28
GG Tau A	T	0.73	2.4	1.5	37 ± 1	$\cdots$	30.31	10.2	14,26,39
GM Aur	T	0.84	1.6	0.74	54 ± 5	$0.221^{+0.082}_{-0.085}$	1.23	12.4	8,14,26,39
HD 141569	HB	2.3	1.7	22.	53 ± 5	1[b]	236	$\cdots$	9,31,32,33
HD 144432	HA	2.	2.0	32.	45	2.1 ± 0.2	$\cdots$	74	9,29
HD 163296	HA	2.30	2.8	30.2	60 ± 5	$0.23^{+0.01}_{-0.02}$	$\cdots$	120	9,21,25,33
HD 190073	HA	4.3	3	83	50^{+30}_{-50}	$0.55^{+0.03}_{-0.06}$	$\cdots$	15	15,18,35
HL Tau	T	0.55	2.2	0.9	55 ± 13	$\cdots$	160	$\cdots$	10,23,28
MWC 480	HA	1.65	1.6	11.5	26 ± 7	0.21 ± 0.002	$\cdots$	85	39, 35
MWC 758	HA	2	2.1	20.6	46	0.28 ± 0.02	$\cdots$	$\cdots$	30,33
RR Tau	HA	2.7	$\cdots$	65	90	$\cdots$	$\cdots$	$\cdots$	24
RY Tau	T	2.37	3.6	7.6	25	0.19 ± 0.01	6.4-9.1	52.2	7,13,14,28
SR 9	T	1.2	2.9	2.7	34 ± 4^{a}	$0.23^{+0.11}_{-0.10}$	3.2	15.8	11,19
Su Aur	wT	1.97	3.5	10.7	52 ± 10	0.18 ± 0.025	0.5-0.6	65	7,13,14
T Tau N	T	2.41	2.8	8.91	29^{+10}_{-15}	0.11 ± 0.004	3.1-5.7	20.1	6,13,14
TW Hya	T	1.0	1	0.25	7 ± 1	0.06 ± 0.01	0.04	4	40,20,34,37,16
VV Ser	HA	2.6	2.4	49	81^{+9}_{-51}	$0.25^{0.30}_{-0.02}$	$\cdots$	229	25,36,36
BP Tau	T	1.24	1.9	0.93	30^{+4}_{-2}	$0.083^{+0.029}_{-0.041}$	2.10	7.8	8,26,14,39
CY Tau	T	0.48	1.6	0.47	47^{+8}_{-8}	0.032	0.56	10	14,26,28,39
DF Tau	T	0.53	3.6	2.97	78^{+12}_{-35}	$\cdots$	17.69	$\cdots$	10, 11, 22
GK Tau	T	0.75	2.3	1.17	53^{a}	$\cdots$	8.99	18.7	12,14, 26
IQ Tau	wT	0.52	2.4	0.65	79	0.045	1.8	11.5	14,28
LkCa 15	T	1.10	0.74	0.74	42 ± 5	$0.099^{+0.034}_{-0.048}$	0.10	12.5	8,14,26,39
UZ Tau E	T	0.47	2.8	1.6	54^{+3}_{-3}	$\cdots$	$\cdots$	15.9	14, 39

[i]T:T Tauri Star; wT: weak-line T Tauri star; HA/HB: HAe/Be Star

[a]$i_\star$ from stellar rotation data

[b]Upper limit

[c]Lower limit

[d]UX Orionis star; we assume $i > 80°$.

References. — (6) Akeson et al. 2002 (7) Akeson et al. 2005a (8) Akeson et al. 2005b (9) van den Ancker et al. 1998 (10) Beckwith et al. 1990 (11) Bouvier 1990 (12) Bouvier 1995 (13) Calvet et al. 2004 (14) Clarke & Bouvier 2000 (15) Cuttela & Ringuelet 1990 (16) de la Reza & Pinzon 2004 (17) Eisner et al. 2003 (18) Eisner et al. 2004 (19) Eisner et al. 2005 (20) Eisner et al. 2006 (21) Grady et al. 2000 (22) Gullbring et al. 1998 (23) Hayashi et al. 1993 (24) Hernandez et al. 2004 (25) Hillenbrand et al. 1992 (26) Johns-Krull 2002 (27) Koerner & Sargent 1995 (28) Kitamura et al. 2002 (29) Leinert et al. 2004 (30) Mannings & Sargent 2000 (31) Marsh et al. 2002 (32) Merin et al. 2004 (33) Monnier et al. 2005 (34) Muzerolle et al. 2000 (35) Pogodin et al. 2005 (36) Pontoppidan et al. (in prep) (37) Qi et al. 2004 (38) Semenov et al. 2005 (39) Simon et al. 2001 (40) Thi et al. 2004